

Aerodynamic and aero-acoustic improvement of electric motor cooling equipment
Vad J., Horváth Cs., Kovács J. G.

Accepted for publication in Proceedings of the Institution of Mechanical Engineers
Part A-Journal Of Power A
Published in 2014
DOI: [10.1177/0957650913517678](https://doi.org/10.1177/0957650913517678)

Aerodynamic and aero-acoustic improvement of electric motor cooling equipment

Proc IMechE Part A:
J Power and Energy
2014, Vol. 228(3) 300–316
© IMechE 2014
Reprints and permissions:
sagepub.co.uk/journalsPermissions.nav
DOI: 10.1177/0957650913517678
pia.sagepub.com



J Vad¹, Cs Horváth¹ and JG Kovács²

Abstract

A radial flow rotor with radially aligned straight blades, used in electric motor cooling, has been considered as datum fan. The aerodynamic performance and acoustic behaviour of the datum fan have been measured, in order to establish a basis for redesign. As replacement for the datum fan, an axial flow shrouded rotor with skewed blades has iteratively been designed, involving computational fluid dynamics and computational aero-acoustics tools. The aim of redesign was reducing fan noise and moderating motor shaft power absorbed by the fan, while retaining the original cooling performance. Special flow features have been taken into consideration in three-dimensional axial rotor design, such as leakage flow in the axial clearance between the rotor shroud inlet and the perforated cover, and strong radial flow as well as deviation due to the motor shield located close downstream. The axial rotor has been manufactured via rapid prototyping. Measurements on the prototype confirmed the achievement of the redesign goal. The effect of axial clearance size on the operation of the axial rotor has been investigated by computational fluid dynamics, computational aero-acoustics and experimental means. It has been pointed out that the axial clearance size is a sensitive parameter in influencing fan aerodynamics and aero-acoustics, for which the major mechanisms, associated with the leakage flow, were qualitatively identified. Both the computational and experimental studies revealed the existence of an acoustically unfavourable clearance size, for which maximum noise emission can be expected. A semi-empirical model was outlined as starting point in prediction of cooling flow rate as a function of axial clearance size as well as other parameters.

Keywords

Electric motor cooling fan, radial flow fan, axial flow fan, leakage flow, noise reduction

Date received: 25 July 2013; accepted: 18 November 2013

Introduction

Electric motors are often cooled by fan rotors attached to the rear end of motor shaft. Examples for typical rotors and the related flow paths are presented in Figure 1. The proportion of dimensions in the sketches does not truly correspond to reality, for better visibility. The air enters the fan via a perforated cover in front of the rotor, directing the cooling air-flow towards the cooling ribs located at the motor circumference. In a traditional layout, the cooling air-flow is generated by a radial flow rotor. The radial rotor is equipped with a back-plate, on which the radially aligned straight blades are installed (Figure 1(a)). After a quasi-axial inlet, the fluid is diverted radially outward along the back-plate, and is redirected toward the axial direction by the cover. Such a radial rotor has the main advantages of having a simple, easy-to-manufacture geometry, and unidirectional operation, i.e. the flow direction does not depend on the direction of rotation. However, the simple blade geometry results in extensive flow

separation, increased aerodynamic loss and pronounced noise.

The electric motors in point often operate in an environment where noise emission is to be limited, e.g. in building service engineering for residential buildings. Furthermore, the available shaft power provided by the motor is desirable to be maximised, in order to improve the competitiveness of the product on the market. Therefore, the manufacturer of the motor may initiate the reduction of noise emitted by the cooling fan, as well as reduction of shaft power absorbed by it, whereas retaining the original cooling

¹Department of Fluid Mechanics, Budapest University of Technology and Economics, Budapest, Hungary

²Department of Polymer Engineering, Budapest University of Technology and Economics, Budapest, Hungary

Corresponding author:

J Vad, Department of Fluid Mechanics, Budapest University of Technology and Economics (BME), Bertalan Lajos u. 4–6, H-1111 Budapest, Hungary.
Email: vad@ara.bme.hu

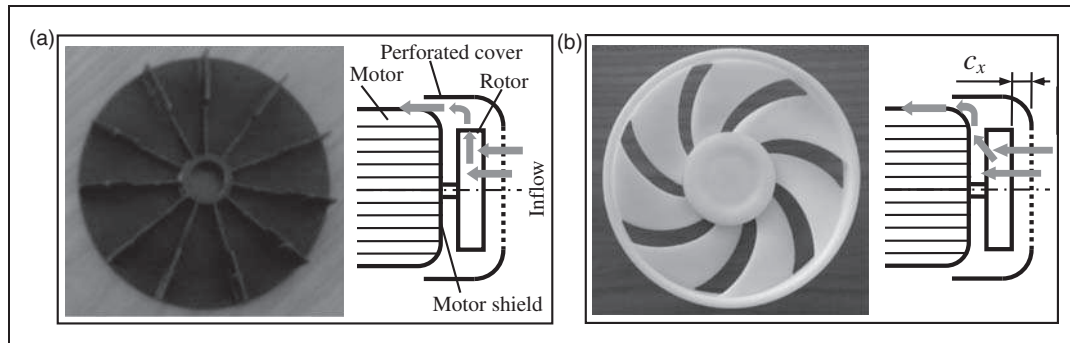


Figure 1. Photo of rotors and simplified meridional scheme of flow paths: (a) radial flow–datum–rotor; (b) axial flow–newly designed–rotor, with indication of axial clearance.

Source: reproduced with permission from Vad et al., 2011.¹²

performance. A possible means is replacing the radial rotor with an appropriate axial flow rotor (Figure 1(b)), as suggested in Borges.¹ In this case, the fluid passes the rotor nearly axially, and is diverted radially outward by the motor shield. If the motor shield is located close downstream of the rotor, a significant radial velocity component already develops inside the rotor.

When designing an axial fan for replacement of an existing radial fan used for motor cooling, a number of aspects, undiscovered in the open literature, are found, as overviewed below.

Only very few publications have reported on electric motor cooling fans.^{1,2} The literature on radial flow rotors with truly radially shaped straight blades, or, in more general, on radial flow blade rows with extremely high incidence, is very limited.^{2,3} Such reports are confined to the brief presentation of rotor geometry,² occasionally supplemented with a basic aerodynamic survey.³ The studies are confined either to acoustic² or to fluid mechanical aspects,³ lacking in the combination of the two. To the authors' best knowledge, no information is available in the open literature on characteristic and efficiency curves of radial flow motor cooling fans.

Aerodynamics- and aero-acoustics-related reports on axial flow automotive cooling fans, operating in a confined environment, may provide valuable information for redesign.^{4–9} However, the results cannot be fully adapted to electric motor cooling fans, due to the following geometrical differences in the confined rotor environment: (i) presence of the perforated inlet cover, (ii) presence of the shield of the electric motor, located extremely close downstream of the rotor. These geometrical constraints influence the three-dimensional (3D) flow field upstream, inside and downstream of the fan blade passages, and such 3D phenomena are to be considered in blade design.

Rotors of industrial axial fans, often incorporated in a ducted configuration, are characterised by a *radial* clearance between the blade tip and the casing wall. The behaviour of flow near the blade tip of the fan rotor, exhibiting a radial clearance, has been a

subject of extensive research.^{10,11} Nevertheless, the axial rotors applied for cooling of electric motors are shrouded, and an *axial* clearance of size c_x is present between the perforated inlet cover and the inlet rim of rotor shroud (see Figure 1(b)). To the authors' best knowledge, the aerodynamic and acoustic effect of axial clearance in electric motor cooling fans has not been studied so far by others.

The authors intend to share their novel experiences gathered in the topics outlined above. The present paper gives a summary on an industrially initiated research and development (R&D) project, aiming at redesigning an existing – datum – radial fan rotor to that of an axial one. To this end, the aerodynamics and acoustics behaviour of the datum radial fan and the newly designed axial fan have experimentally been investigated. For the axial rotor, special attention has been paid to the effect of axial clearance size. The design and survey of the axial rotor has been aided by a validated computational fluid dynamics (CFD) tool, supplemented with computational aero-acoustics (CAA) simulation. Basic fluid mechanical considerations have also been involved while elaborating a semi-empirical model for prediction of leakage flow rate through the axial clearance. The geometrical, measurement and computational details of the fans are disclosed herein in a limited manner, for confidentiality reasons. Preliminary studies in the topic of the paper were published in Vad et al.^{12,13}

Survey on the radial flow datum fan

The datum radial fan rotor is presented in Figure 1(a). The characteristics of the radial fan are summarised in Table 1. The rotor has been subjected to aerodynamic and acoustic experimentation in the built-in configuration, in order to establish a target operational point and quantitative guidelines for redesign. The test rig, capable for characteristic curve and efficiency measurements, is presented in Figure 2. Although the fan operates only in one particular operating point in a given set-up, extensive characteristic curves have been measured, in order to provide optional information

on how the fan can collaborate with various perforated inlet covers of various aerodynamic resistances. The atmospheric pressure is measured by means of a digital barometer. A high-pressure fan of variable speed, serving as a booster fan, supplies air to the system. In order to win over the losses in the facility, the application of this booster fan is obligatory for measuring operational states at which the total pressure upstream of the perforated cover is atmospheric – as in the real operational state. The cooling volume flow rate q_C is measured by means of a flow metering pipe with a built-in standardised through-flow orifice meter.¹⁴ The differential pressure on the orifice meter is measured by means of a digital manometer, calibrated to an officially certified Betz micromanometer. The air moves from the orifice meter pipe to a measurement pipe, fitting to the diameter of the cooling fan cover, and connected to it in a gastight manner. Preliminary studies revealed the following: (i) the measurement pipe causes negligible departure from the realistic inlet condition, being that of a free inlet which sucks air from the surroundings; (ii) the orifice meter does not cause any detectable disturbing effect in the measurements taken in the measurement pipe upstream of the cooling fan. The temperature in the measurement pipe is measured by a calibrated resistance thermometer. The two-pole asynchronous electric motor operates without loading on the front end of the motor shaft (idle running). The air sucked from the measurement pipe through the perforated cover is exhausted over the cooling ribs. The motor speed is measured on the shaft by means of a digital stroboscope. The mechanical power input to the cooling fan is estimated from the measured motor speed, with knowledge of the high-resolution motor characteristic

curve (mechanical power delivered by the motor as a function of speed). The operational state of the cooling fan is adjusted by the speed of the booster fan.

The fan total pressure rise has been obtained as follows

$$\Delta p_t = p_{t \text{ down}} - p_{t \text{ up}} \quad (1a)$$

$p_{t \text{ down}}$ has been estimated with use of the following relationship

$$p_{t \text{ down}} = p_a + \rho \frac{\bar{v}_{x \text{ down}}^2}{2} \quad (1b)$$

In equation (1b), the static pressure has been taken as atmospheric pressure p_a , considering that the blow-out is to the atmosphere. Furthermore, since the cooling ribs eliminate the swirling component of the outlet velocity, the dynamic pressure has been calculated from $\bar{v}_{x \text{ down}}$, the axial mean velocity downstream of the fan. $\bar{v}_{x \text{ down}}$ has been derived as q_C divided by the blow-out cross section at the outlet of the perforated cover.

$p_{t \text{ up}}$ has been estimated as follows

$$p_{t \text{ up}} = p_{t \text{ pipe}} - \Delta p'_{\text{cover}} \quad (1c)$$

For equation (1c), the total pressure in the measurement pipe, $p_{t \text{ pipe}}$, has been obtained as the static pressure measured in the measurement pipe upstream of the cooling fan cover, plus $\rho \bar{v}_{x \text{ up}}^2 / 2$. The static pressure upstream of the cooling fan cover, relative to the atmospheric pressure, has been measured in the measurement pipe, three pipe diameters upstream of the cover. This pressure was measured through four static pressure taps connected to a common piping, by means of a digital manometer also calibrated to the Betz meter. $\bar{v}_{x \text{ up}}$ has been derived as q_C divided by the measurement pipe cross section. The static pressure drop through the perforated cover, $\Delta p'_{\text{cover}}$, was measured during a separate experiment, by using the facility presented in Figure 2, but excluding the motor, and driving the air through the perforation by means of the booster fan.

Table 1. Radial fan characteristics.¹²

N	11
Re	$1.51 \cdot 10^5$
Ma	$5.29 \cdot 10^{-2}$
Φ_n	0.123
Ψ_n	0.322

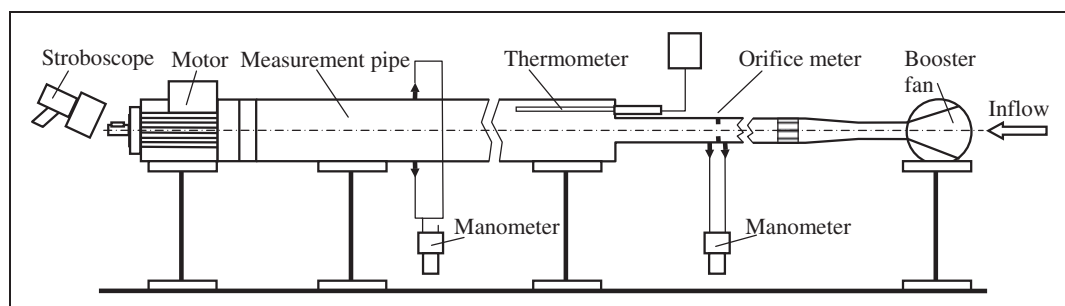


Figure 2. Scheme of facility for characteristic curve and efficiency measurement for the radial flow datum fan.¹²

The experimental uncertainty has been estimated according to the instructions e.g. in ISO 5167-1:2003 and ISO 5167-2:2003,¹⁴ with consideration of propagation of errors, for the vicinity of the nominal operating state used in redesign. The study of Vad et al.^{15,16} are given as references for uncertainty estimates. Table 2 summarises the absolute uncertainty of the measurement-based dimensionless quantities appearing in the paper, valid at a 95% confidence level. Whenever visible, the uncertainty ranges in Table 2 are indicated in the diagrams in the paper, using error bars over the entire measurement range.

Considering the nominal geometrical data, the nominal axial clearance between the inner surface of the perforated cover and the front enveloping plane of the radial rotor is $\approx 0.2d_t$. Experimental data on the radial rotor are presented in the paper for this nominal clearance. The axial clearance may slightly be modified due to manufacturing and assembling tolerances. Based on preliminary experiments, it has been considered that the size of the axial clearance has only a minor effect on the behaviour of the radial rotor at usual operation.

Figure 3 presents the measured characteristic and efficiency curves of the radial rotor. In the real environment, the cooling fan sucks air from the motionless ambient air field, having total pressure being equal to

the atmospheric pressure. Therefore, the nominal operational state of the fan is imitated in the test facility when the total pressure in the upstream measurement pipe is just equal to the atmospheric pressure. Accordingly, the nominal operational state has been identified at the flow rate of Φ_n at which $p_{t \text{ pipe}} - p_a = 0$, i.e. $\Psi_S(\Phi)$ takes zero value. The corresponding point on the $\Psi(\Phi)$ characteristic curve, i.e. $\Psi_n(\Phi_n)$, specified in Table 1, serves as a basis for redesign.

The total efficiency η_t has been calculated as follows

$$\eta_t = \frac{\Delta p_t q_C}{P} \quad (2)$$

It has been considered that

$$\eta_t = \eta_h \eta_V \quad (3)$$

The isentropic total pressure rise $\Delta p_{t \text{ is}}$ has been estimated on the basis of the Euler equation of turbomachinery, with consideration of slip factor correction judged in Lakshminarayana¹⁷ (p. 126, Fig. 2.43) to be reasonably accurate for impeller blades having radially aligned trailing edge (TE). The hydraulic efficiency η_h has been obtained as follows

$$\eta_h = \frac{\Delta p_t}{\Delta p_{t \text{ is}}} \quad (4)$$

The volumetric efficiency has been defined as follows

$$\eta_V = \frac{q_C}{q_R} \quad (5)$$

With use of the calculated η_t and η_h data, the volumetric efficiency η_V has been calculated on the basis of equation (3) as $\eta_V = \eta_t / \eta_h$.

As suggested in Figure 3, the estimated η_V data increases nearly linearly with the flow rate. The more the Φ the less the throttling on the fan; the more the η_V the lesser will be the inclination of

Table 2. Absolute experimental uncertainty.

Location	Quantity	Uncertainty
Figure 3	Φ	$\pm 1 \times 10^{-3}$
Figure 3	Ψ	$\pm 3 \times 10^{-3}$
Figure 3	Ψ_S	$\pm 3 \times 10^{-3}$
Figure 3	η_t	$\pm 2 \times 10^{-2}$
Figure 8(b)	$\Delta \tau$	$\pm 3 \times 10^{-3}$
Figures 9(a) and 10	c_x/d_t	$\pm 4 \times 10^{-3}$
Figure 9(a)	Φ_C/Φ_0	$\pm 5 \times 10^{-2}$
Figure 10	SPL	± 0.5 dB

SPL: sound pressure level.

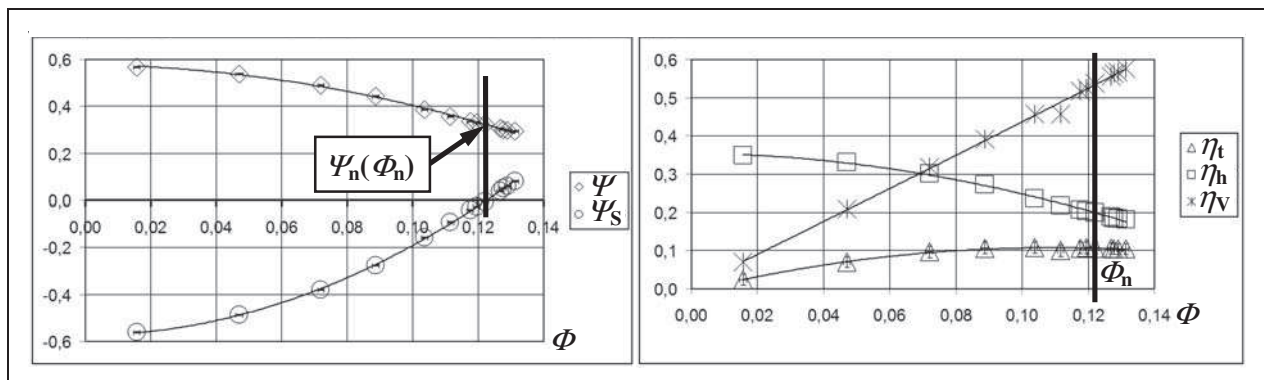


Figure 3. Performance curves of the datum radial fan. Left: characteristic curves, right: efficiency curves.¹²

the fan for reverse leakage flow in the clearance between the rotor and the cover. The η_v values vary within the approximate range of 0–0.6. These values are relatively low in comparison to usual radial fan arrangements (e.g. $\eta_v=0.94$ in Carolus,¹⁸ p. 129). This implies that the volumetric loss, associated with the reverse leakage flow, plays a major aerodynamic role in the judgement of fan operation. Therefore, special attention will be paid to the leakage flow in fan redesign. It is also marked that the η_h values vary within the approximate range of 0.2–0.35, and are relatively low in comparison to usual radial fans (e.g. $\eta_h=0.83$ in Carolus,¹⁸ p. 129) owing to the blade geometry being far from aerodynamic optimum.

Acoustical investigations were carried out on the datum radial fan, for the idle running state of the motor, in the reverberation chamber of the Georg von Békésy Acoustic Laboratory, operated by the Department of Fluid Mechanics, BME. The aim of these studies was to point out the main sources of noise generation. The applied instrumentation was a Brüel&Kjaer 4133 microphone and a Brüel&Kjaer PULSE 3109 type data acquisition system. The measurements were carried out in accordance with the standard.¹⁹ The following configurations are discussed herein: (a) motor alone (without fan rotor and without cover), (b) motor with both fan rotor and cover, as shown in the sound pressure level (SPL) spectra in Figure 4. The SPL values have been presented in the figure in comparison to a representative basic level. Only the 0 to 3.2 kHz range is presented for better visibility. The noise of the electromotor is principally generated by mechanical (unbalance, roller bearing, etc.) and magnetic (magnetostriction) components. The noise signature is indicated in the spectra by tonal components, which peak out of the broadband noise at approximately 50 and 100 Hz and their harmonics.

The spectra confirm the dominance of fan noise, underlining the possibilities for noise reduction via redesigning the fan. The fan rotor is characterised by broadband noise extending to some kilohertz.

No remarkable tonal noise is dedicated to the fan. This behaviour meets the expectations given that the set-up does not provoke the appearance of remarkable classic tonal noise sources. That is, the rotor blades are non-uniformly spaced (see Figure 1(a)) for moderation of ‘steady loading noise’, also termed as Gutin noise.¹⁸ Furthermore, no remarkable stator (e.g. guide vane) elements are present, contributing to elimination of ‘unsteady loading noise’ due to any rotor–stator interaction.¹⁸ On the basis of the discussion by Carolus,¹⁸ it is assumed that the detected broadband fan noise is dominated by wake, boundary layer and separation noise sources, in accordance with the aerodynamic drawbacks of the applied blade geometry. From the perspective of axial fan design, the following conclusions have been drawn from the acoustic survey. (i) Blade skew is to be incorporated in the design¹⁸ for suppressing the tonal fan noise further on. Having applied the blade skew, no further efforts are planned for study and moderation of tonal noise. (ii) Instead, the acoustic design and the supporting CAA tool are to focus on *broadband* noise sources (BNS). (iii) Attention is to be paid to possible moderation of noise related to the leakage jet, blade wake and boundary layers – even subjected to separation – by appropriate design.

CFD and CAA technique for the axial rotor

The design process has been aided by CFD as well as by CAA means. As the investigation has been initiated by an industrial R&D project of strict schedule, the use of a quick and cost-effective means of investigation is necessary. Earlier experiences in successfully applying Reynolds-averaged Navier–Stokes (RANS) steady-state CFD simulations in combination with BNS models²⁰ has encouraged the use of this investigative method here as well. No concerted CFD and CAA data have preliminarily been available for axial flow electric motor cooling fans. Therefore, the use of relatively easy and quickly accessible, yet fairly effective, CFD and CAA methods, involving

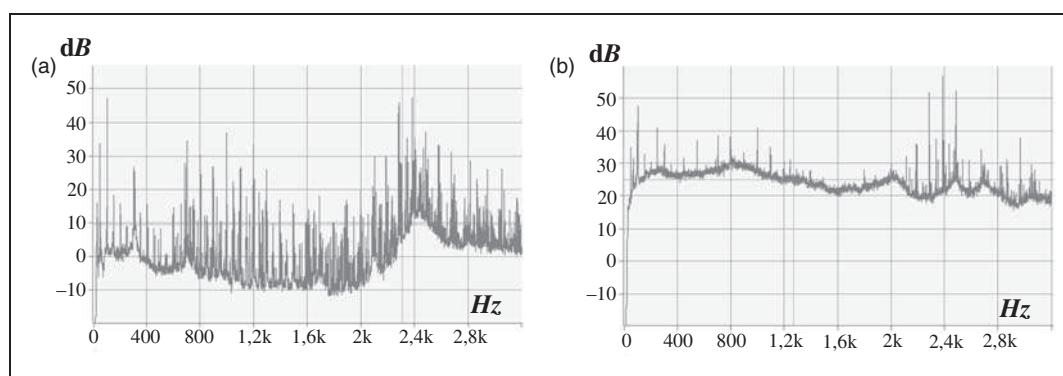


Figure 4. Measured SPL spectra: (a) motor alone; (b) motor with radial flow rotor and cover.¹²

commercially available software tools, was judged as being a significant contributor to the State-of-the-Art in the design and analysis of such fans. Steady flow simulations were carried out using the finite-volume CFD code ANSYS Fluent.²¹ The CFD tools available in ANSYS Fluent have repeatedly been used to successfully simulate turbomachinery in similar applications, as can be seen in Borges.¹ Prior to axial rotor modelling, validation studies were carried out on the basis of the radial rotor. The literature on turbomachinery CFD simulations²² as well as previous experiences^{12,13} have shown that from among the available two-equation turbulence models, the $k-\omega$ SST model is expected to provide the best fit to experimental results in this application. This was confirmed in the radial rotor investigations, and therefore this turbulence model has been used in the axial rotor simulations.

Sensitivity studies were carried out on setting the extension of the blow-out zones to various sizes. In the final CFD model, independence from the blow-out zone size has been achieved. At the sides of the blow-out zone, the boundary condition was 'pressure-outlet'. Figure 5 presents the computational domain. Taking periodicity into consideration, the computations regarded only one blade pitch. Utilising the features of the annular cascade configuration, boundary conditions of periodicity were applied. The inlet face is a sector of a virtual cylindrical inlet pipe, corresponding to the measurement pipe in Figure 2, with a central angle of $360^\circ/N$. Downstream of the inlet face, sectors of the fan cover and the rotating hub, with one blade in the middle of the domain, are included. At the inlet face, located upstream of the fan casing, within the suction pipe, a steady pressure inlet is defined. The inlet turbulence intensity has been set to 10% and the hydraulic diameter was set to the diameter of the virtual cylindrical inlet pipe, in order to reproduce former experimental experiences. The perforated part of the inlet cover is reproduced using a porous material. Approximately 50% of the cells are located in the refined domain in the vicinity of the blade. The computational domain embedding the rotor was composed from meshes of two different types, in order to achieve the best grid quality with a fast

mesh generation process. A proper block structured mesh was generated around the blade O-grid. On the shroud and hub faces, boundary layer meshes were applied. ANSYS BladeGen and ANSYS TurboGrid were used to generate and mesh the adjacent domains of the blade. The quality of the mesh was checked using the built-in checker of ANSYS TurboGrid and by means of validation calculations. The mesh in the blade passage domain, termed 'passage-domain mesh' was created only once, and, using ANSYS Fluent non-conformal interfaces,²¹ was connected to the mesh of the surrounding domain of each case. The geometry of the surrounding domain was based on the passage-domain mesh and was extrapolated from it. A proper block structured mesh was generated with the aid of H-type boundary and shear layer mesh resolution. Four geometries were developed with different axial clearance sizes by means of ANSYS ICEM. A good mesh quality and the adequate positioning of the interfaces were basic requirements. The skewness of the cells in the surrounding domains was below 0.8. The volume change and aspect ratios also confirmed the good quality of the mesh. The mesh can be characterised by a value of $y^+ < 3$ and an orthogonal quality greater than 0.25. At the non-conformal interfaces, the cell sizes were synchronised. The interfaces were planar faces and were placed as far as possible from the observed areas. The two non-continuous meshes were connected numerically with the aid of the non-conformal interfaces. A multiple reference frame model was used during the simulations in modelling the rotation of the moving walls. Typical computations required approximately 14,000–17,000 iterations. The solutions were considered converged when the scaled residuals of all equations were resolved below the levels of order of magnitude of 10^{-3} and the surface monitors remained practically constant. Journal files were used in automating the calculations. The speed of revolution of the moving walls was gradually increased to the operational speed, and then the porous zones representing the perforated fan cover and the cooling ribs were switched on.

The cooling flow rate for the axial rotor is derived as follows

$$q_C = q_R - q_L \quad (6)$$

Since both q_R and q_L are sensitive to the axial clearance size – as will be demonstrated later –, the axial clearance-dependent cooling flow rate has been judged as a representative indicator of validity of the CFD tool. Therefore, for CFD validation, the computed cooling flow rate, i.e. flow rate delivered toward the cooling ribs, being equal to the inlet flow rate through the perforation of the front cover, being dependent on the axial clearance size, was compared to experimental data. The computed and measured cooling flow rate values are presented later

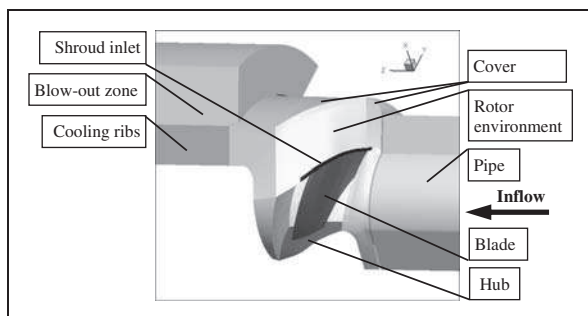


Figure 5. Details of computational domain.¹³

in Figure 9(a). The error bars correspond to the experimental uncertainty. The fair quantitative agreement between the CFD and experimental data, along with the proper resolution of the trend of decreasing flow rate with increasing clearance size, support the validity of the CFD tool.

The data presented in Figure 9 but not discussed so far will be referred to in section ‘Semi-empirical model for flow rate prediction’.

For obtaining qualitative acoustic information on the effect of axial clearance size, ANSYS CAA tools for localising BNS, which are based on the steady CFD results, and which have already been applied in Horváth and Vad,²⁰ have been used. In using BNS models, statistical turbulence quantities computed from RANS results, in conjunction with semi-empirical correlations and Lighthill’s acoustic analogy, can give information as to the source of the broadband noise.²¹ The acoustic source terms on the walls have been estimated on the basis of boundary layer parameters, as well as in the free shear layers. In this way the source terms can be used to find the locations of the noise sources and also compare them, which shows that BNS models provide useful means by which the prominent noise generating regions in a flow domain are determined. Furthermore, BNS models give a means by which different variations of a design can be compared in order to screen out noisier variations and identify the primary sources of the noise.^{23,24} The application of this CAA methodology to industrial axial fans has been inspired e.g. by the study of Cros and Carbonneau.²⁵

Axial fan design

Aerodynamic design aspects

The following section briefly outlines the methodology and the guidelines applied to the combined, iterative aerodynamic design and ‘sound design’¹⁸ of the axial flow fan by which the datum radial fan is to be replaced. The design goal was to provide a cooling performance represented by the datum radial fan. The iterative modifications resulted in the final axial fan geometry presented in Figure 1(b). During the redesign, the rotor environment – i.e. perforated inlet cover, motor shield, outlet to the cooling ribs – had to be left unchanged, according to the instructions of the industrial partner.

Considering the low Mach number in Table 1, incompressible flow has been considered in fan redesign. The $[\Phi_n, \Psi_n]$ data presented in Table 1 were taken as initial design data. Figure 6 presents the data couple of diameter and speed factors $[\delta, \sigma]$ in the Cordier diagram,¹⁸ calculated with use of the $[\Phi_n, \Psi_n]$ data in Table 1. The figure suggests that the redesign target could be realised by means of a mixed flow fan – higher flow turning capability – rather than by means of an axial rotor. Still, an axial rotor was

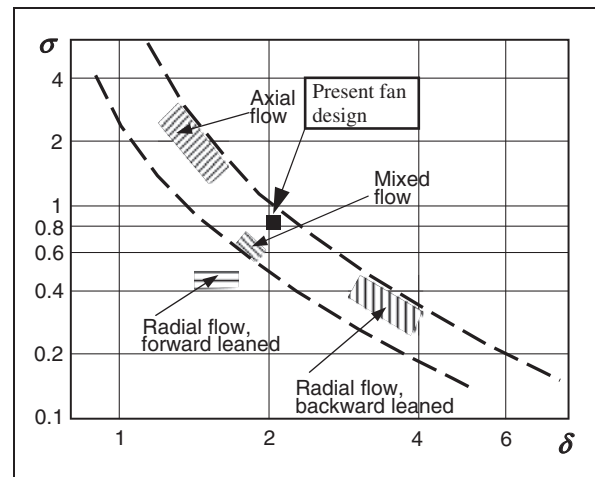


Figure 6. Cordier diagram.

Source: reproduced with permission from Vad et al., 2011.¹²

selected for the final configuration, according to the instructions of the industrial partner, given that it can be mass-produced by means of a significantly more simple injection moulding device. The demand for relatively high flow turning forecasts the challenge of designing an axial flow fan of relatively high blade load. Highly loaded blades are assumed to have an increased inclination to generate broadband noise such as boundary layer and separation noise. Special attention is to be paid to control such noise sources in rotor design.

$N=7$ has been chosen for the axial fan. An odd number was intended to be taken for the blade count, in order to moderate any apparent noise originating from the interaction of the blades with the four supporting elements of the perforated cover. The eventually chosen blade count is a compromise between (1) having possibly the least number of blades, for manufacturing simplicity, and for maximising the chord-based Reynolds number, and (2) moderating the axial extension of the rotor, according to the limitation in the available space, by applying more blades of moderate axial chord. The controlled vortex design (CVD) technique,^{16,26} prescribing spanwise increasing blade circulation along the blade height, has been applied. The benefits of the CVD method in the present design assignment are as follows. (i) The blade sections at higher radii are better utilised, generating locally higher axial velocities. This fits to the circumstance that the cooling fan should perform dominantly at outer radii, near the location of the cooling ribs. (ii) The increased performance contribution of blade sections at higher radii also matches the demand of high specific performance (see the Cordier diagram in Figure 6). (iii) In order to moderate the fan noise, the rotor circumferential speed is to be limited.¹⁸ At a prescribed performance, this can be carried out only by means of CVD, i.e. by better utilisation of blade sections at higher radii. (iv) Near the hub, the stall and aerodynamic blockage are expected to be

pronounced, due to the presence of the hub and the motor shield.⁴ By means of CVD, the hub diameter can be purposefully reduced, and near-hub blade sections can be unloaded, leading to the moderation of near-hub loss.

The blade geometry has iteratively been designed, with consideration of the CFD results obtained for the various geometries. The CFD-based design has been carried out for a nominal axial clearance, being representative from manufacturing and assembling points of view. The leakage flow occurring in the nominal axial clearance influences the incidence to the leading edge (LE), the 3D interblade flow, and the flow deviation past the TE. Such effects are to be taken into account in design, by adjusting the camber line geometry.

In preliminary design, the air velocity data has been correlated with linear cascade measurements on the basis of the reference by Wallis.²⁷ Blade sections of circular arc camber line and of uniform thickness, with a rounded LE and TE, have been applied. This simple geometry is beneficial from manufacturing point of view. Furthermore, at the low *chord-based* Reynolds number, valid for the present case, such blade sections show better aerodynamic performance than profiled blade sections.¹⁸ During the design process, the direction of the blade LE has been adjusted for achievement of favourable incidence, for moderation of the apparent near-LE separation even at presence of leakage flow.

In the preliminary design state, the effect of downstream blockage, caused by the vicinity of the motor shield, has approximately been considered on the basis of Gifford et al.⁴ and Hunt et al.⁵ Compared to flow deviation correlations valid for linear cascades,²⁸ significantly increased flow deviation from the blade TE direction was experienced in the CFD

studies, caused by the vicinity of the downstream blockage (motor shield). This has been compensated for, by increasing the flow turning capability of the blading. The interblade flow has been found to be characterised by a radial velocity occasionally reaching the order of magnitude of that of axial velocity. Accordingly, the blade sections were designed by modelling conical stream tubes through the rotor.

Acoustic design aspects

It has been considered that if the blade tip Mach number is below approximately 0.1, an axial fan without guide vanes can be expected to be less noisy than a radial fan.¹⁸ In order to moderate the fan noise, the rotor circumferential speed has slightly been moderated¹⁸ by reducing d_t in comparison to the radial rotor. Circumferential forward skew ('sickle-shaped' blades) has been applied for suppressing the tonal noise, and for reducing the broadband boundary layer (and any apparent separation) noise, thanks to a thinner boundary layer on the suction side of the highly-loaded blades as well as for achieving aerodynamic improvements. These guidelines were suggested in Carolus.¹⁸ When aerodynamically harmonising the non-radial blade stacking geometry with the CVD concept, guidelines reported in Vad²⁶ have been taken into consideration.

Axial fan prototyping

The prototype fan has been manufactured at the Department of Polymer Engineering as outlined in Figure 7. The designed rotor has been printed on an Objet Alaris 30 rapid prototyping machine, using a durable thermoset material. The used polyjet technology applies a layer thickness of 28 μm , which allows

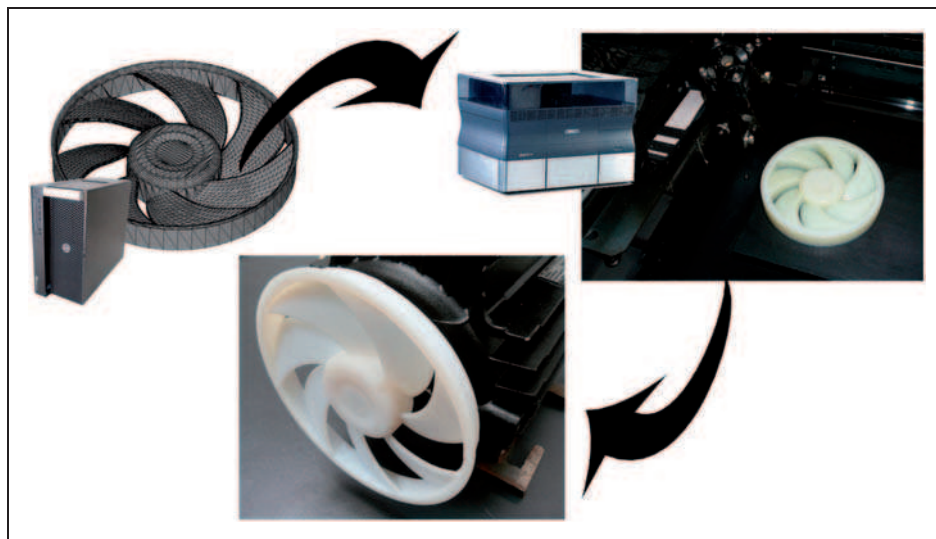


Figure 7. Production chain for prototyping: designing of the rotor with CAD; data transfer via stl file; 3D printing with Objet Alaris 30; assembly.

for a fine surface finish and reduces the need for post-processing. From the final CAD design the time required for the first test was less than one day. The fan was prototyped for both possible directions of motor rotation (compare Figures 1(a) and (7)).

Discussion of experimental results

As approved by the industrial partner, the experimental work involving the axial rotor and presented in the paper has been restricted to the activities reported below. The estimated experimental uncertainties are reported either in Table 2 or in the text. For the comparative measurements between the radial and axial fans, the nominal axial clearance has been set for the axial rotor.

Radial and axial fans: Comparative thermal camera measurements

In order to judge the cooling performance of the competing fans, measurements were carried out using a Testo 875-2 thermal camera, with the aid of the Department of Polymer Engineering, BME, in idle run of the electric motor, starting from the same initial state. A representative warm-up process is shown in Figure 8. It was found that the ‘hot spot’ of the highest temperature is a proper quantitative indicator of the warm-up process over the entire cooling rib zone, selected as the interrogation area. Quantification of the colour scale was intentionally left non-disclosed.

The figure confirms that the axial rotor has achieved the design goal: its cooling performance is identical to that of the radial one, within the range of experimental uncertainty.

Radial and axial fans: Comparison of absorbed shaft power; efficiency estimates

It has been concluded from the test measurements that the shaft mechanical power P absorbed by the

axial fan is 70% of that of the radial fan, within the uncertainty range of $\pm 5\%$. Considering identical fan performance, this implies a total efficiency of $\approx 1.5\eta_t$ in comparison to the radial fan. Taking representative mean values for Φ_C/Φ_0 and Φ_R/Φ_0 on the basis of data ranges in Figure 9(a) and (b) (discussed later), and considering equation (5), a pessimistically estimated representative mean volumetric efficiency of $\eta_V = (\Phi_C/\Phi_0)/(\Phi_R/\Phi_0) \approx 0.65$ has been calculated for the axial rotor. Taking equation (3) into account, a representative mean hydraulic efficiency η_h has been calculated as $\eta_h = \eta_t/\eta_V$ for the axial fan. The comparative efficiency data are presented in Table 3. The values estimated for the radial fan are taken from Figure 3. It must be kept in mind that the efficiency data are rough estimations. Still, they suggest the qualitative trend of improvement of both volumetric and hydraulic efficiencies by fan redesign. The efficiency data estimated for the axial rotor are far below the values being valid for regular ducted axial fan layouts (e.g. $\eta_V = 0.98$, $\eta_h = 0.80$, in Carolus,¹⁸ p. 136). This underlines the challenges and demonstrates the possibilities of further improvement of axial fan design for electric motor cooling.

Radial and axial fans: Comparative overall noise measurements

Comparative acoustic measurements were carried out in idle run. The acoustic measurements were carried out with use of a SVANTEK 959 sound and vibration analyser, supplemented with a SVANTEK SV12L preamplifier, GRAS 40AE condenser microphone and SVANTEK SA22 wind protection sphere. The equipment was calibrated by a SVANTEK SV30A piezo-electric microphone calibrator. The motor was mounted on a vibration damping board. Three measuring points were taken for each studied case. The base point was taken as fitting to the axis of rotation, on the outer surface of the fan cover. The three measuring points were taken on a horizontal plane, at a

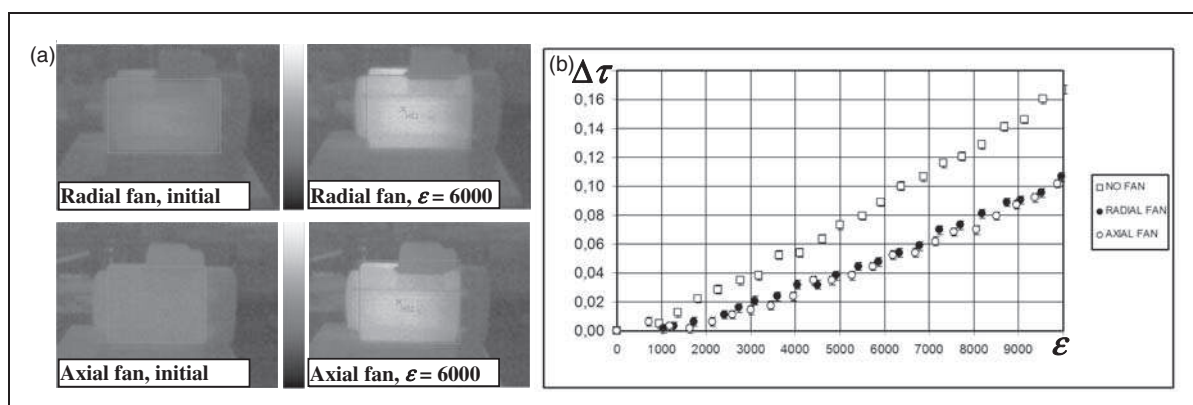


Figure 8. Thermal camera studies: (a) examples for thermal camera records; (b) warm-up history. Source: reproduced with permission from Vad et al., 2011.¹²

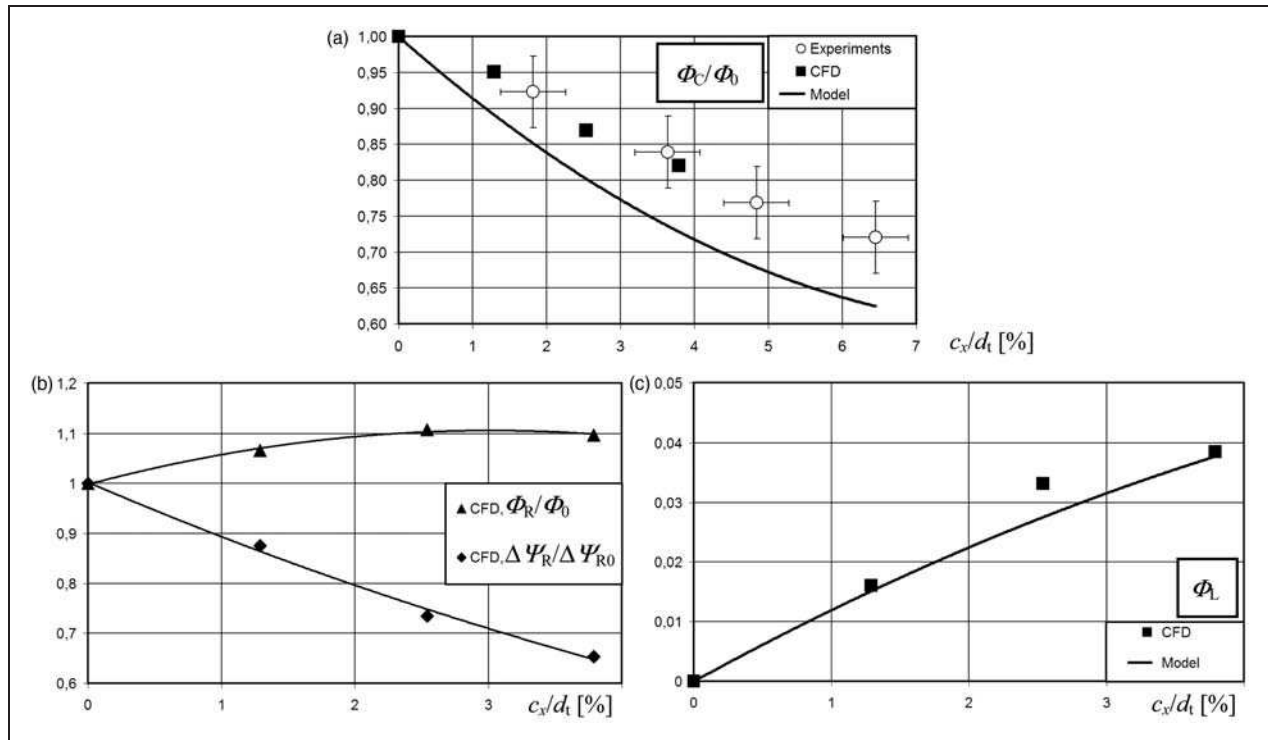


Figure 9. Trends due to change of axial clearance size: (a) Measured, computed and semi-empirically modelled cooling flow rate; (b) computed rotor flow rate and pressure difference; (c) computed and semi-empirically modelled leakage flow rate.¹³ CFD: computational fluid dynamics.

Table 3. Representative approximate shaft power and efficiency data.

	Radial fan	Axial fan
P	P	$0.7P$
η_t	0.11	0.17
η_v	0.55	0.65
η_h	0.2	0.25

distance of 0.50 m from the base point: one point on the axis of rotation, and two side points in a $\pm 90^\circ$ off-axis arrangement. The noise of the electric motor without rotor and cover was also measured, and its effect was extracted from the evaluation. The experimental uncertainty, dedicated mainly to repeatability error due to positioning uncertainty of the microphone, caused the variance of measurement data within a 1 dB range. The measurements revealed a 7 dB(A) reduction of the A-weighted SPL for the axial rotor, averaged for the three points, in comparison to the datum radial rotor.

Axial fan: Measurements on axial clearance-dependent cooling flow rate

The cooling flow rate has been obtained from turbine anemometer data collected in a measurement pipe upstream of the perforated cover. The results are presented in Figure 9(a), in the form of Φ_C/Φ_0 , as

function of c_x/d_t . The measurements reveal that the axial clearance size has a significant impact on the cooling flow rate.

Axial fan: Measurements on axial clearance-dependent noise

The radiated noise has been measured for various axial clearance sizes. The Optinav Inc., Array 24 phased array microphone system, operated by the Department of Fluid Mechanics, has been used for performing beamforming studies on the cooling fan arrangements. The application of this measurement system in another turbomachinery-related departmental study has been published in Benedek and Tóth.²⁹ The results of the beamforming studies are under processing, and are planned to be reported in a separate paper. This paper is confined to reporting data obtained only by a selected single microphone incorporated in the phased array microphone system. It has been assumed that the noise associated with the axial clearance-related phenomena can mostly propagate toward the air field upstream of the inlet cover via the perforation. Therefore, the microphone axis has been aligned on the rotor axis for the measurements presented herein. The microphone has been set to the distance of 0.36 m from the cover. Measurements were made with and without the fan being mounted on the axis. The noise measured in the case with the removed fan is referred to as background noise. Figure 10 presents the measured SPL

values relative to the background noise data, for various clearances. The figure indicates that the axial clearance size influences the fan noise. It also suggests the existence of an intermediate clearance size for which maximum noise is generated. A third-order polynomial trend line has arbitrarily been fitted to the data points, with the intention of making the trend more visible. Among others, this non-monotonous trend will be investigated in a detailed manner in the next section.

Discussion of CFD and CAA results

As indicated by the experimental data in Figures 9(a) and 10, the axial clearance size influences the aerodynamic as well as acoustic behaviour of the axial rotor. For a comprehensive explanation on the underlying physics, CFD and CAA data are presented herein on the axial rotor for four axial clearance

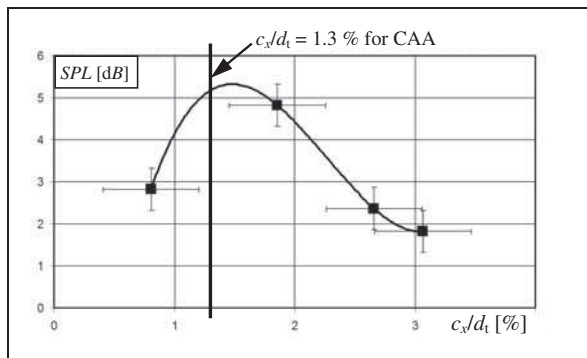


Figure 10. Measured SPL data, relative to the background noise, for various axial clearances. SPL: sound pressure level; CAA: computational aero-acoustics.

sizes of $c_x/d_t = 0\%$ (zero clearance), 1.3%, 2.5% and 3.8%. The CFD and CAA plots are shown in the sequence of axial clearance increasing from left to right.

Figure 11 presents the plots of computed absolute velocity magnitude and acoustic power level over a planar inlet section of the computational domain. The interrogation plane is perpendicular to the axis of rotation, and is located at the entrance of the cylindrical inner surface of the shroud, downstream of the rounded inlet rim of the shroud. The arch-shaped white zone in the plots corresponds to the cross section of the shroud. At zero clearance, the interrogation plane coincides with the inner surface of the cover at the lowest and the highest radii, and therefore, no computational data are presented for these regions for zero clearance. The figure demonstrates that the leakage velocity peak and leakage flow rate become higher as the axial clearance increases (upper row). The turbulent leakage jet appears as a dominant source of noise in the interrogation plane (lower row).

A more comprehensive explanation can be given on the clearance-related phenomena with use of the absolute tangential velocity, turbulent kinetic energy, and acoustic power level plots over a longitudinal section, as seen in Figure 12. The interrogation plane is parallel to the axis of rotation and intersects the blade near the tip LE (the blade is viewed in the figure). The upper limit of the scale of the tangential velocity (white colour) corresponds to u_t . The inlet fluid flowing nearly axially through the perforated cover interacts with the rotating inlet rim of the shroud. The tangential velocity plots (uppermost row) reveal that this interaction results in a rotating separation zone. The nearly radially inward leakage flow tends to intensify the detachment of flow from the inlet rim

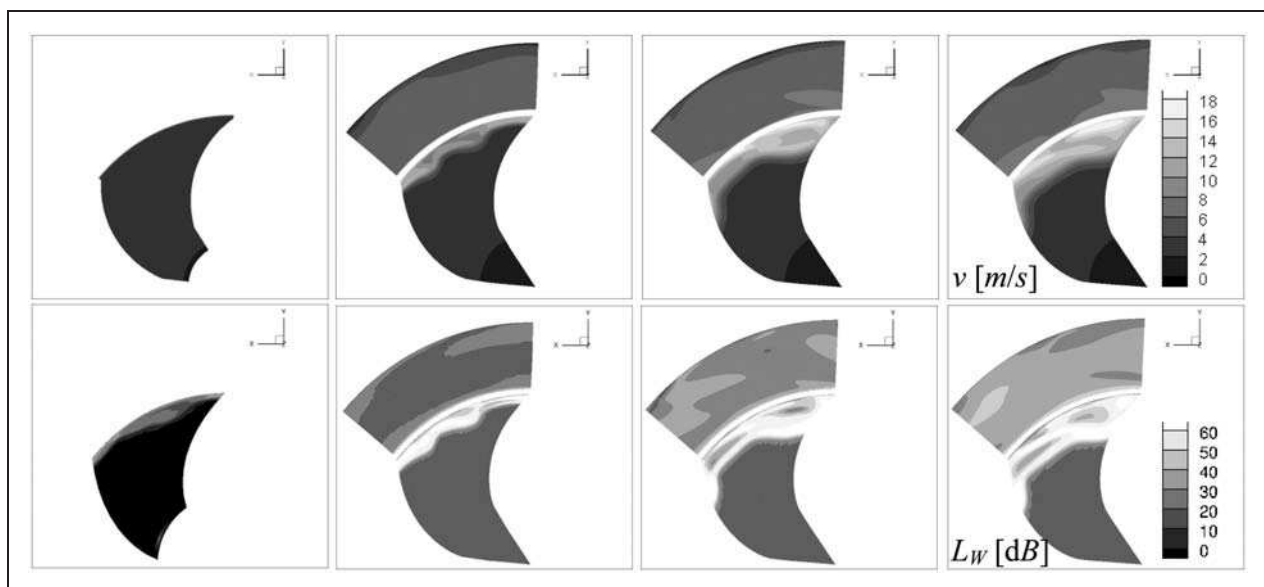


Figure 11. Viewing the inlet section of the computed domain from the axial direction. Axial tip clearance increasing from left to right. Upper row: magnitude of absolute velocity; Lower row: acoustic power level.¹³

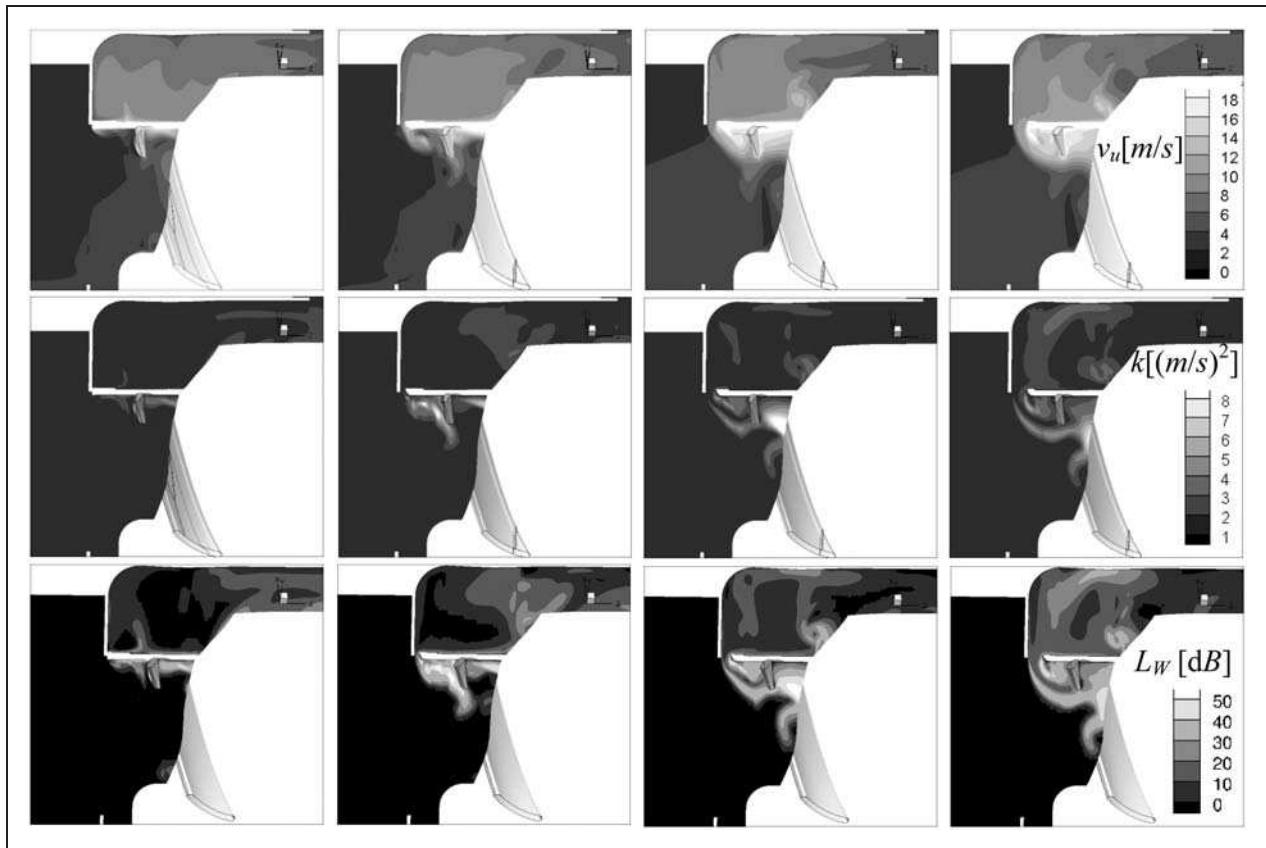


Figure 12. Longitudinal section of computed domain. Axial tip clearance increasing from left to right. Upper row: tangential component of absolute velocity; Middle row: turbulent kinetic energy; Lower row: acoustic power level.¹³

of the shroud. The larger the clearance the more intense the leakage flow, the more extended the rotating separation zone, and the higher the magnitude of rotation. At the largest clearance, the k plot (fourth plot in the middle row) demonstrates the presence of two separate zones of high turbulence past the clearance: (i) the shear layer at the interaction between the leakage flow and the inlet flow through the cover, (ii) the rotating separation zone, bounded by the leakage flow. As the clearance size decreases, these two zones tend to get closer, and, at a certain clearance size, they are merged. This merging phenomenon results in extremely high local k values, and, accordingly, an absolute maximum in the local acoustic power level (second plots from the left in the middle and lowermost rows). Although Figure 11 suggests that the leakage flow noise tends to intensify with increasing clearance size, the lowermost row in Figure 12 draws to our attention that this trend is not monotonous: the locus of absolute maximum of sound power is present in the CAA plot of the intermediate clearance size of $c_x/d_t = 1.3\%$. This observation is in accordance with the measurement data in Figure 10 in which the maximum noise appears near the clearance of $c_x/d_t = 1.3\%$, investigated by CAA, as indicated in the figure.

The impact of the near-clearance phenomena on blade aerodynamics and blade aero-acoustics can be

viewed in Figures 13 and 14. In Figure 13, the static pressure over the blade pressure surface, relative to a reference pressure, is plotted. According to the presence of the rotating separation zone upstream of the LE, the incidence angle of the relative flow to the blade decreases, and so does the blade load. This results in reduced static pressure values near the LE on the pressure side, in the radial region where the rotating separation zone affects the flow incidence. The larger the clearance size the more reduced the pressure near the LE, due to a more pronounced effect of the rotating separation zone and the more extended the low-pressure region toward lower radii.

In Figure 14, the static pressure, relative to a reference pressure, as well as the acoustic power level over the blade suction surface, is presented. The blade unloading effect due to the rotating separation zone, affected by the clearance size, is also visible here in the static pressure diagrams. At zero clearance (upper row, first plot), a pronounced suction effect is visible near the LE, followed by an adverse pressure gradient as one moves toward the TE. In the suction side blade tip-shroud corner, near the LE, a zone of nearly constant static pressure can be detected. This suggests the presence of a separation zone that is probably due to local blade overloading caused by the negative dihedral.³⁰ Increasing the clearance, the suction effect and the adverse pressure gradient,

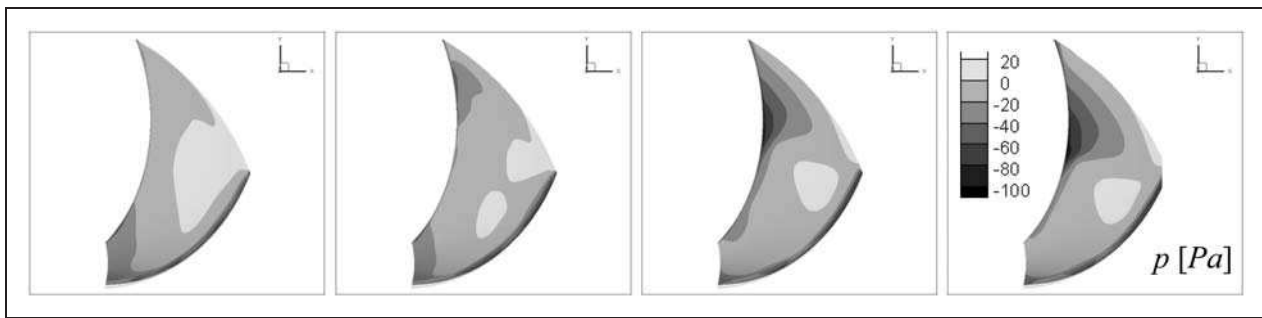


Figure 13. Pressure surface of blade. Axial tip clearance increasing from left to right. Static pressure, relative to a reference value.¹³

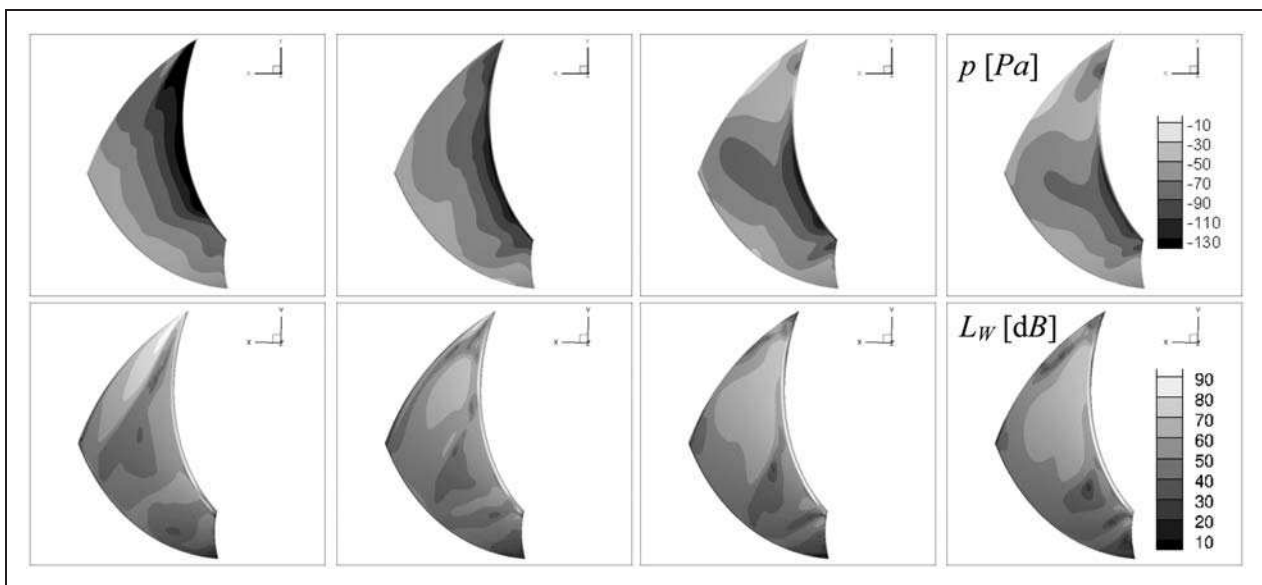


Figure 14. Suction surface of blade. Axial tip clearance increasing from left to right. Upper row: static pressure, relative to a reference value; Lower row: surface acoustic power level.¹³

manifesting the blade load, tend to decrease, and tend to confine to lower radii. As seen in the acoustic power level plot for zero clearance (lower row, first plot), the separation zone near the tip LE appears as a source of peak noise. As the clearance increases, the leakage flow tends to energise the separation zone. As a result, the noise associated with the separation zone is moderated. The zone of highest acoustic power level tends to extend toward lower radii, with lower values of maximum surface acoustic power level.

The observations related to the acoustic power level plots in Figures 11, 12 and 14 suggest the existence of an acoustically unfavourable intermediate clearance size for which maximum noise emission can be expected. This is in accordance with the measurement data in Figure 10.

Semi-empirical model for flow rate prediction

A semi-empirical model is intended to be developed for prediction of volumetric loss associated with the

leakage flow, i.e. leakage flow rate, and for prediction of cooling flow rate. A preliminary version of the model is documented herein. This model can contribute to performance prediction during the design of axial fans used for electric motor cooling.

Δp_R is the difference between mass-averaged static pressures downstream and upstream of the rotor. According to the blade unloading effect discussed using Figures 13 and 14, Δp_R is expected to decrease with increasing clearance. This trend can be observed in the CFD-based $\Delta\Psi_R/\Delta\Psi_{R0}$ plots in Figure 9(b). An exponential trend line fits the data points well, as presented in the figure. The related exponential function is used in further modelling, fulfilling the asymptotic condition of $\Delta p_R \rightarrow 0$ if $c_x/d_t \rightarrow \infty$.

The fluid rotates in the clearance. The front wall of the clearance, i.e. the cover, is motionless. The rear wall of the clearance, i.e. the inlet rim of the shroud, rotates at an angular speed ω . As a first approximation, it has been assumed that the fluid in the clearance rotates at a mean angular speed of $\omega_{\text{mean}} = \omega/2$. A radial pressure gradient develops in the clearance.

The resultant pressure difference Δp_ω acts against Δp_R in driving the leakage flow. Δp_ω is expressed from the following approximate relationship, based on the radial component of Euler equation

$$\begin{aligned} \frac{\partial p}{\partial R} &= \frac{\Delta p_\omega}{\Delta R} = \rho \frac{v_{u\text{mean}}^2}{R_{\text{mean}}} = \rho R_{\text{mean}} \omega_{\text{mean}}^2 \\ &= \rho \left(\frac{d_t}{2} + \frac{\Delta R}{2} \right) \left(\frac{\omega}{2} \right)^2 \end{aligned} \quad (7)$$

The pressure difference driving the leakage flow is as follows

$$\Delta p_L = \Delta p_R - \Delta p_\omega \quad (8)$$

It is assumed on the basis of the Bernoulli equation that a leakage flow of velocity v_L develops through the clearance

$$v_L = \sqrt{\frac{2\Delta p_L}{\rho}} \quad (9)$$

It can be shown that the hydraulically equivalent diameter of the clearance, taken as 4 times the mean cross section in the clearance divided by the wetted circumference (over the two peripheries of the clearance), is $2 c_x$.

The leakage flow is contracted in the clearance. The contraction coefficient C_C , being dependent on $2 c_x$ and ΔR (i.e. diameter and length of a hydraulically equivalent cylindrical Borda mouthpiece) is approximated on the basis of Dong and Lienhard.³¹

The leakage flow rate is predicted as follows

$$q_L = 2 R_{\text{mean}} \pi c_x C_C v_L \quad (10)$$

Figure 9(c) makes a comparison between the leakage flow rate data supplied by the CFD tool as well as predicted using the semi-empirical model ('Model' in the figure). Despite the simplifying assumptions made in the model, a fair agreement is observable.

The cooling flow rate is to be calculated according to equation (6). As shown in Figure 9(b), q_R varies with the clearance size. At this preliminary state of semi-empirical modelling, q_R is taken briefly as $q_R \equiv q_0$. This implies, considering equation (6), the following approximation

$$q_C = q_0 - q_L \quad (11)$$

The semi-empirically modelled cooling flow rate is presented in Figure 9(a) ('Model' in the figure). Although the trend of flow rate decrease is fairly well represented by the model, it gives a conservative (pessimistic) estimation on the cooling flow rate: the data obtained from the model are below the measured ones. The following ways of improving the model are envisaged, in the sequence of anticipated importance:

(i) Semi-empirical modelling of q_R , instead of the approximation of $q_R \equiv q_0$, in equation (6) (conf. Figure 9(b)). (ii) A more accurate consideration of C_C in equation (10). (iii) An appropriate extension of Bernoulli equation, represented in equation (9), to friction losses, e.g. loss at clearance inlet to the clearance. (iv) A more accurate consideration of effect of rotation in the clearance, instead of the approximation of $\omega_{\text{mean}} = \omega/2$ in equation (7). The model improvement is to be based on further CFD studies, focussing on the aforementioned details.

Summary

A CFD- and CAA-based iterative design has been carried out in order to obtain an axial fan replacing the radial fan used presently for electric motor cooling, in order to reduce fan noise and absorbed mechanical power, whereas retaining the original cooling performance. The paper outlines the purposeful, problem-specific 3D controlled vortex design of the axial fan blades. Testing of the datum radial rotor and the axial rotor was carried out with the incorporation of aerodynamic, energetic, thermodynamic and acoustic experiments. The measurements revealed an approximately 30% reduction of absorbed mechanical power and an approx. 7 dB(A) reduction of the A-weighted sound pressure level for the axial rotor, relative to the radial one, while the cooling performance remained unchanged. The novelty content of the paper is summarised as follows.

1. Extending the measurement-based experience on radial fans, the characteristic and efficiency curves – including total, hydraulic and volumetric efficiencies – have been presented for a radial rotor with radially adjusted straight blades, incorporated in an electric motor cooling layout. Both η_h and η_v were found to be relatively low in comparison to usual radial fan arrangements. η_v was found to increase nearly linearly with volume flow rate. This reflects the trend, that the lower the throttling of the fan, the lower the inclination of the fan to have reverse flow in the clearance between the rotor and the cover.
2. Adding to the open literature on axial fans, detailed CFD and broadband-noise CAA data have been reported for the redesigned axial rotor, for various axial clearances between the perforated inlet cover and the inlet rim of the rotor shroud. This data plays a primary role in the investigation of axial rotor aerodynamics and acoustics in an electric motor cooling layout.
3. Based on the CFD data, the following comprehensive explanation has been given on the mechanisms through which the size of axial clearance size affects the aerodynamic performance of the axial fan. The fluid entering via the perforated cover interacts with the rotating inlet rim of the

shroud. This results in a rotating separation zone. The inward leakage flow tends to intensify the detachment of flow from the rim. The rotating separation zone causes a moderation in flow incidence angle to the blades, and thus, moderation in blade load and in pressure rise occurs. The larger the axial clearance size, (i) the more intense the leakage flow rate, leading to deterioration of cooling flow rate, (ii) the higher the rotation and larger the extension of the rotating separation zone, and (iii) the more pronounced the effect of deteriorating the flow incidence to the blades, the blade load, and the pressure rise.

4. With concerted evaluation of the CFD and CAA data, the leakage flow-related noise generation phenomena have been investigated, such as (i) noise of the turbulent leakage flow, being intensified with axial clearance size, (ii) emergence of high-turbulence regions (shear layer at the inlet, rotating separation zone), apparently causing a maximum in the local acoustic power level at an intermediate clearance size, (iii) noise related to a separation zone in the blade tip-shroud corner over the suction surface, being attenuated with axial clearance size. Based on these studies, and confirmed by measurements, it has been concluded that an acoustically unfavourable intermediate axial clearance size exists, for which maximum noise emission can be expected.
5. A preliminary version of a semi-empirical model has been elaborated, with the aid of the CFD studies, for prediction of clearance size-dependent flow rate. The model fairly well predicts leakage flow rate. The model provides a conservative (pessimistic) prediction on the cooling flow rate. The way for further developing the model has been outlined.

Acknowledgements

Gratitude is expressed to Grundfos Hungary Manufacturing Ltd. for initiating and funding the presented R&D project, as well as for permitting to the publication of this paper. The reported results are acknowledged by the authors as independent scientific results incorporated in the doctoral programme of Cs. Horváth. Gratitude is expressed to the co-authors of the preliminary study;¹² to Dr G. Szabó for contributing to prototyping and to the thermocamera measurements; to Mr G Kiss for assisting the CFD studies; and to Mr R Budafoki and Mr L Vitai for giving assistance in developing the semi-empirical model.

Funding

This study was supported by the Hungarian National Fund for Science and Research under contracts of No. OTKA K 63704 and K 83807. The work relates to the scientific programme of the project 'Development of quality-oriented and harmonised R + D + I strategy and the functional model at BME', supported by the New Hungary Development Plan (Project ID: TÁMOP-4.2.1/B-09/1/KMR-2010-0002). It is

also supported by the project 'Talent care and cultivation in the scientific workshops of BME' project (Project ID: TÁMOP-4.2.2/B-10/1-2010-0009).

References

1. Borges SS. CFD techniques applied to axial fans design of electric motors. In: *Proceedings of the international conference on fan noise, technology and numerical methods (FAN2012)*, Senlis, France, 18–20 April 2012.
2. Noda S, Mizuno S and Suzuki K. Fan noise and resonance frequency analysis in fan-cooled induction motor. In: *Proceedings of the first international symposium on advanced technology of vibration and sound, VSTech 2005*, Hiroshima, Japan, 1–3 June 2005, pp. 41–46.
3. Johnson G, Simmons K and Foord C. Experimental investigation into windage power loss from a shrouded spiral bevel gear. *ASME Paper No. GT2007-27885*, 2007.
4. Gifford NL, Savory E and Martinuzzi RJ. Experimental study of automotive cooling fan aerodynamics. *SAE Paper No. 2007-01-1525*, 2007.
5. Hunt AG, Savory E, Gifford NL, et al. Downstream blockage corrections of automotive cooling fan module performance. *SAE Paper No. 2009-01-0175*, 2009.
6. Henner M, Moreau S and Brouckaert JF. Comparison of experimental and numerical flow field in an automotive engine cooling module. In: *Proceedings 8th European conference on turbomachinery fluid dynamics and thermodynamics (ETC'08)*, Graz, Austria, 23–27 March 2009, pp. 387–399.
7. Verstraete T, Roytta P, Henner M, et al. Design and off-design optimization of a fan for automotive applications. In: *Proceedings of the 9th European conference on turbomachinery fluid dynamics and thermodynamics (ETC'9)*, Istanbul, Turkey, 2011, pp. 1485–1496.
8. Zayani M, Çağlar Ş and Gabi M. Aeroacoustical investigations on axial fans for automotive cooling systems. In: *Proceedings of the international conference on fan noise, technology and numerical methods (FAN2012)*, Senlis, France, 18–20 April 2012.
9. Henner M, Demory B, Beddadi Y, et al. Low weight, high speed automotive fan design by 3D inverse method. In: *Proceedings of the 10th European conference on turbomachinery fluid dynamics and thermodynamics (ETC'10)*, Lappeenranta, Finland, 15–19 April 2013, pp. 404–414.
10. Corsini A, Rispoli F and Sheard AG. Aerodynamic performance of blade tip end-plates designed for low-noise operation in axial flow fans. *ASME J Fluids Eng* 2009; 131.
11. Bianchi S, Corsini A, Rispoli F, et al. Far-field radiation of tip aerodynamic sound sources in axial fans fitted with passive noise control features. *ASME J Vib Acoust* 2011; 113: 051001-1:051001-11.
12. Vad J, Horváth Cs, Lohász MM, et al. Redesign of an electric motor cooling fan for reduction of fan noise and absorbed power. In: *Proceedings of the 9th European conference on turbomachinery fluid dynamics and thermodynamics (ETC'9)*, Istanbul, Turkey, 21–25 March 2011, pp. 69–79.
13. Vad J and Horváth Cs. Study on the effects of axial clearance size on the operation of an axial flow electric motor cooling fan. In: *Proceedings of the 10th European conference on turbomachinery fluid dynamics and*

- thermodynamics (ETC'10)*, Lappeenranta, Finland, 15–19 April 2013, pp. 543–552.
14. Standards ISO 5167-1:2003 and ISO 5167-2:2003. *Measurement of fluid flow by means of pressure differential devices inserted in circular cross-section conduits running full*. Geneva, Switzerland: ISO, 2003.
 15. Vad J, Kwedikha ARA and Jaberg H. Effects of blade sweep on the performance characteristics of axial flow turbomachinery rotors. *Proc IMechE, Part A: J Power and Energy* 2006; 220: 737–751.
 16. Vad J, Kwedikha ARA, Horváth Cs, et al. Aerodynamic effects of forward blade skew in axial flow rotors of controlled vortex design. *Proc IMechE, Part A: J Power and Energy* 2007; 221: 1011–1023.
 17. Lakshminarayana B. *Fluid dynamics and heat transfer of turbomachinery*. New York: John Wiley & Sons, Inc., 1996.
 18. Carolus T. *Ventilatoren*. Wiesbaden: B. G. Teubner Verlag, 2003.
 19. Standard ISO 3743-2:1994. *Acoustics – Determination of sound power levels of noise sources – Engineering methods for small, moveable sources in reverberant fields*. Geneva, Switzerland: ISO, 1994.
 20. Horváth Cs and Vad J. Broadband noise source model acoustical investigation on unskewed and skewed axial flow fan rotor cascades. In: *Proceedings of the conference on modelling fluid flow (CMFF'09)*, Budapest, Hungary, 9–12 September 2009, pp. 682–689.
 21. ANSYS 13.0 Fluent. *User's guide*. Canonsburg, PA: ANSYS, Inc., 2010.
 22. Tannoury E, Khelladi S, Demory B, et al. Influence of blade compactness and segmentation strategy on tonal noise prediction of an automotive engine cooling fan. *Appl Acoust* 2013; 74: 782–787.
 23. Stanko TS, Ingham DB, Fairweather M, et al. Computational fluid dynamic prediction of noise from a cold turbulent propane jet. *ASME Paper No. GT2008-50834*, 2008.
 24. Wagner C, Hüttl T and Sagaut P. *Large-eddy simulation for acoustics*. Cambridge: Cambridge University Press, 2007.
 25. Cros S and Carbonneau X. Computational study of the aerodynamic impact of stall margin improvements in a high tip speed fan. In: *Proceedings of the 8th European conference on turbomachinery fluid dynamics and thermodynamics (ETC'08)*, Graz, Austria, 23–27 March 2009, pp. 401–410.
 26. Vad J. Incorporation of forward blade sweep in preliminary controlled vortex design of axial flow rotors. *Proc IMechE, Part A: J Power and Energy* 2012; 226: 462–478.
 27. Wallis RA. *Axial flow fans and ducts*. New York: John Wiley & Sons, 1983.
 28. Lieblein S. Experimental flow in two-dimensional cascades. In: *Aerodynamic design of axial-flow compressors*. Report NASA SP-36, Washington DC, 1965.
 29. Benedek T and Tóth P. Beamforming measurements of an axial fan in an industrial environment. *Periodica Polytechnica, Mech Eng Ser* 2013; 57(2): 37–46.
 30. Vad J. Aerodynamic effects of blade sweep and skew in low-speed axial flow rotors at the design flow rate: An overview. *Proc IMechE, Part A: J Power and Energy* 2008; 222: 69–85.
 31. Dong W-g and Lienhard JH. Contraction coefficients for Borda mouthpieces. *ASME J Fluids Eng* 1986; 108: 377–379.

Appendix

Notation

c_x	axial clearance between the inlet rim of shroud and the perforated cover (m)
C_C	coefficient of contraction
d_t	blade tip diameter (m)
k	turbulent kinetic energy (m^2/s^2)
L_W	acoustic power level (dB)
Ma	tip Mach number: u_t per speed of sound in air at 20°C
N	blade count
p	static pressure (Pa)
p_t	total pressure (Pa)
Δp_L	pressure difference driving the leakage flow (Pa)
$\Delta p'_{\text{cover}}$	static pressure drop through the perforated cover (Pa)
Δp_R	difference of mass-averaged static pressures downstream and upstream of the rotor (Pa)
Δp_t	total pressure rise (Pa)
Δp_ω	static pressure difference through the clearance in radial direction, due to rotation (Pa)
P	shaft power input (W)
q	volume flow rate (m^3/s)
R	radius, radial coordinate (m)
ΔR	radial extension of clearance (m)
Re	Reynolds number: $u_t \cdot d_t$ divided by air kinematic viscosity at 20°C
u_t	blade tip circumferential velocity at nominal speed (m/s)
v	absolute velocity (m/s)
v_L	leakage flow velocity (m/s)
v_u	tangential component of absolute velocity (m/s)
\bar{v}_x	area-average of axial component of absolute velocity (m/s)
y^+	wall normal cell size (in wall units)
δ	diameter factor = $\Phi^{-0.5} \cdot \Psi^{0.25}$ at (nearly) the best efficiency point
ε	normalised time: time (s) multiplied by rotational frequency (Hz) at nominal speed
η_h	hydraulic efficiency
η_t	total efficiency
η_V	volumetric efficiency: η_t/η_h
ω	angular speed of the rotor (1/s)
Φ	flow coefficient: volume flow rate / ($u_t \cdot d_t^2 \cdot \pi/4$)

Ψ	total pressure rise coefficient: mass-averaged total pressure rise/ $(\rho \cdot u_t^2/2)$	down	downstream of rotor
$\Delta\Psi_R$	rotor static pressure difference coefficient: $\Delta p_R/(\rho \cdot u_t^2/2)$	is	isentropic condition
Ψ_S	suction total pressure coefficient: (mass-averaged total pressure upstream of the fan in the measurement pipe minus atmospheric pressure)/ $(\rho \cdot u_t^2/2)$	L	leakage volume flow rate: leaking back through the axial clearance
ρ	fluid density (kg/m^3)	mean	mean value in the clearance
σ	speed factor = $\Phi^{0.5} \cdot \Psi^{-0.75}$ at (nearly) the best efficiency point	n	nominal condition of the radial fan (Figure 3, Table 1), to be used in redesign
$\Delta\tau$	normalised temperature change: temperature change \times air isobar specific heat \times air mass flow rate/motor nominal shaft power, for Φ_n , at 20°C	pipe	in the measurement pipe
		R	rotor volume flow rate: flowing through the rotor
		up	upstream of rotor
		0	reference condition for the axial fan obtained in CFD simulation for zero axial clearance

Subscript

a	atmospheric (ambient) condition
C	cooling volume flow rate: flow rate delivered toward the cooling ribs, representing the cooling performance